Appl. Phys. A
DOI 10.1007/s00339-014-8756-x

Applied Physics A
Materials Science & Processing

Hydroxyethylammonium maleate (HEAM) single crystal for optical limiting applications

N. Sudharsana · S. Hamad · S. Venugopal Rao · V. Krishnakumar · R. Nagalakshmi

Received: 5 June 2014 / Accepted: 27 August 2014

Abstract A novel hydroxyethylammonium maleate single crystal was grown by slow evaporation solution method for the first time. The structure of the title compound is determined by single crystal X-ray diffraction. The linear optical properties were studied using ultraviolet–visible and photoluminescence spectroscopy. The third-order nonlinear optical property of title compound was studied by Z-scan technique to determine its nonlinear absorption and nonlinear refraction. Thermal property was studied by thermogravimetry, differential thermal analysis and differential scanning calorimetric analyses. The mechanical stability of the material was studied by Vickers microhardness tester. Further, etching study was done to examine the defects in the crystal.

1 Introduction

Dicarboxylic acids have been attracting immense interest due to their wide-ranging applications. Generally, the mono-anions of dicarboxylic acids form hydrogen bonded chain. These hydrogen bonds have been used to construct molecular building blocks with structures in both one and two dimensions. The maleates are of practical importance because of their use as coatings with specific properties, efficient catalysts and are also of medicinal significance [1]. Some of the organic compounds of maleate such as L-arginine maleate dihydrate [2], L-phenylalaninium maleate [3], L-alaninium maleate [4], L-arginine formomaleate [5] and a 2-aminopyridinium maleate [6] were reported to have better NLO efficiency than KDP. Generally, optical limiting property exhibited by organic molecules is related to high delocalization of the π-electrons. The optical limiting behavior resulting from nonlinear absorption can occur due to reverse saturable absorption, two-photon absorption, nonlinear refraction and nonlinear scattering [7]. Unlike second-order materials, there exist no molecular symmetry restrictions for the observance of a third-order nonlinear optical response. A minimum of three states (ground state and two excited states) are necessary to characterize the third-order response adequately [8]. In the present work, the new salt, namely hydroxyethylammonium maleate (HEAM), was synthesized and grown. The maleic acid plays a role in hydrogen bond donor with ethanolamine to form HEAM complex. In this work, we report on an experimental investigation of the nonlinear absorption coefficient (two- and three-photon absorption) and nonlinear refractive index of HEAM using picosecond (ps) Z-scan technique at the wavelength of 800 nm by Ti:sapphire (Ti:Sa) laser. The grown crystal was further subjected to various characterization techniques to study its structural, optical, thermal and mechanical properties for the first time in the literature.

N. Sudharsana · R. Nagalakshmi (✉)
Department of Physics, National Institute of Technology, Tiruchirappalli 620015, India
e-mail: nagaphys@gmail.com

S. Hamad
School of Physics, University of Hyderabad, Prof. C.R. Rao Road, Hyderabad 500046, India

S. Venugopal Rao
Advanced Center of Research in High Energy Materials (ACRHEM), University of Hyderabad, Prof. C.R. Rao Road, Hyderabad 500046, India

V. Krishnakumar
Department of Physics, Periyar University, Salem 636011, India

Published online: 25 October 2014

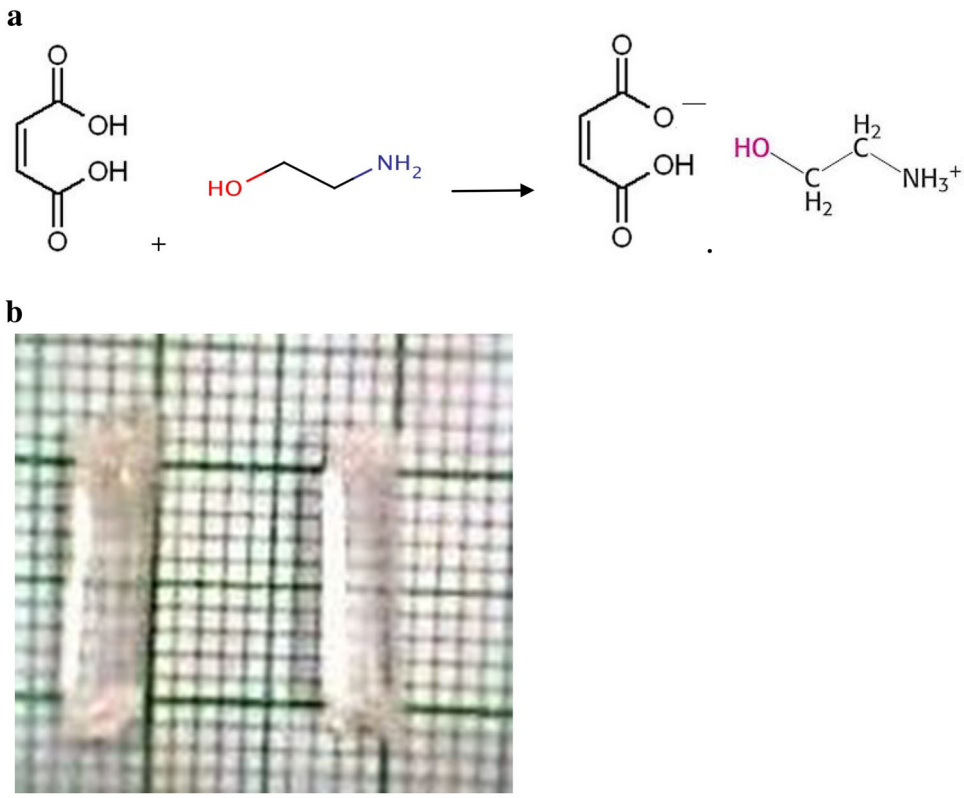

Fig. 1 **a** Reaction scheme of HEAM. **b** Image of as-grown HEAM crystal

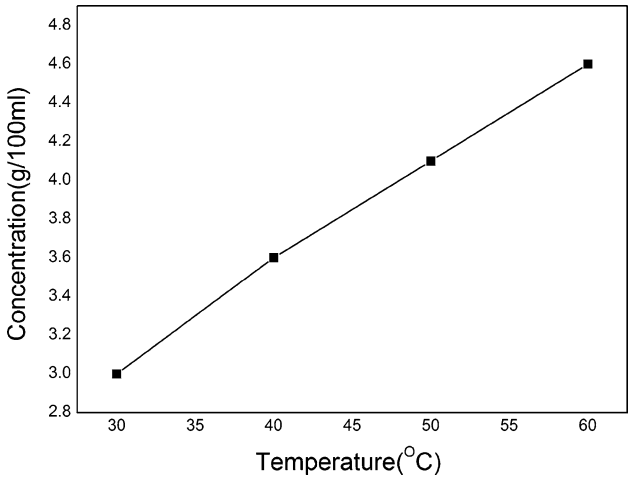

Fig. 2 Solubility curve of HEAM

2 Experimental section

2.1 Synthesis and crystal growth

The HEAM was synthesized by the reaction of maleic acid and ethanolamine (Merck ≥98 %) in ethanol in 1:1 molar ratio at room temperature and stirred for about 30 min over a magnetic stirrer. The white precipitate was collected and then recrystallized from ethanol. The reaction scheme of the HEAM is shown in Fig. 1a. Good quality transparent colorless crystals were harvested after 1 week of evaporation. The as-grown crystal photo with dimension 13 × 3 × 1 mm^3 is shown in Fig. 1b. The pH of the crystal was found to be 6.48.

2.2 Solubility

The solubility was measured using ethanol for four different temperatures from 30 to 60 °C (Fig. 2). The title salt was added to the solvent up to the saturation level. The solvent was completely evaporated by drying the petridish containing the solution. The amount of the salt present in the solution was measured by subtracting the empty petridish weight. The titled compound exhibits positive temperature coefficient of solubility.

2.3 Characterization

Hydroxyethylammonium maleate crystal was subjected to single crystal X-ray diffraction (XRD) analysis using Enraf (Bruker) nonius CAD4 diffractometer with MoK_{α} (0.71073 Å) radiation. The absorption spectrum was recorded using the instrument Shimadzu UV 1700 pharma spectrophotometer in the range 200–1,000 nm with the crystal thickness 2 mm. The photoluminescence (PL) spectrum was recorded using the Jasco spectrofluorometer with xenon lamp as excitation source at room temperature. The thermogravimetry/differential thermal analysis (TG/DTA) study was

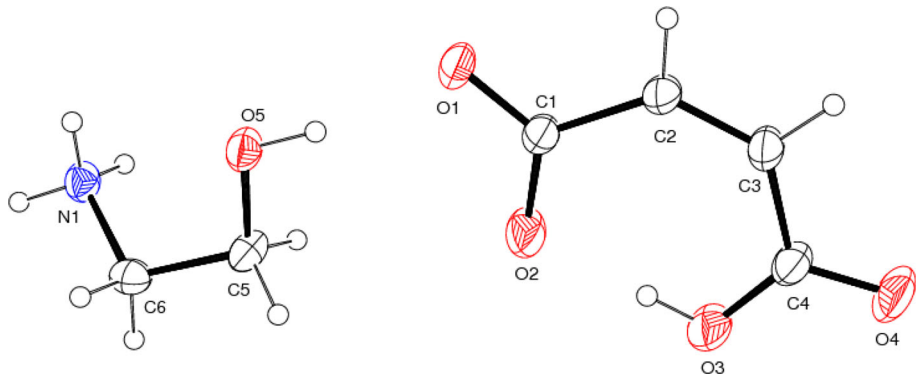

Fig. 3 ORTEP diagram of HEAM single crystal

carried out in the argon atmosphere in the 30–1,000 °C region at a heating rate of 20 °C min^{-1} using thermal analyzer (SII Nanotechnology Inc., Japan, EXSTAR 6200 TG/DTA). The differential scanning calorimetry (DSC) was carried out in the range of 30–500 °C in the argon atmosphere at a heating rate of 10 °C/min using NETZSCH DSC 204. The initial weight of the sample taken for TG/DTA and DSC analyses were 3.5 mg and 4.08 mg, respectively. Due to more scattering centers in the grown crystal, Z-scan experiment was done with the sample dissolved in ethanol and placed in 1-mm glass cuvette. The Z-scan experiment was performed with a picosecond (ps) pulses generated by Ti:sapphire laser at a repetition of 1 kHz with a pulse duration of ~2 ps at 800 nm. The amplifier was seeded with ~15 fs pulses from an oscillator. The input laser beam was spatially filtered to obtain a pure Gaussian profile in the far-field. Z-scan study was performed by focusing the 3-mm diameter input beam using a 200-mm focal length convex lens. The sample was scanned using a high resolution translation stage and the detector (Si PD, SM1PD2A, Thorlabs) output was coupled to a lock-in amplifier. The Z-scan study was performed with solution having concentration of typically 1 mM providing 90 % linear transmittance at 800 nm. Closed aperture scans were performed at low peak intensities (the value of $\Delta\phi$ estimated in all the cases was $<\pi$). The complete details of the Z-scan experiments were reported in our earlier works [9–13]. The Vickers microhardness test was performed on (011) plane by static indentation test at room temperature using Shimadzu HMV-G Micro Vickers hardness test fitted with a diamond indenter. Etching study was carried out using Euromex polarizing microscope with 10 × objective.

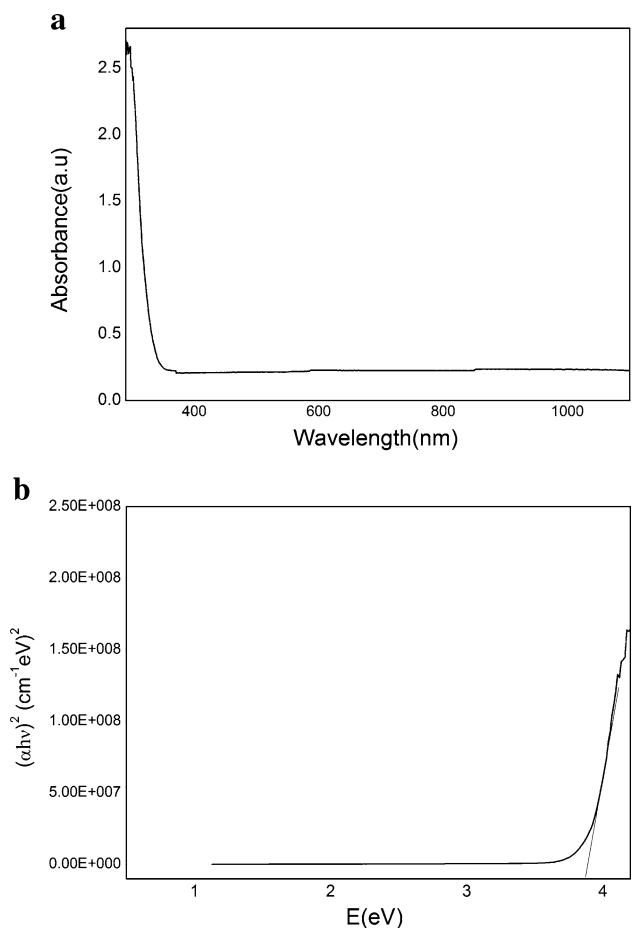

Fig. 4 **a** UV–Vis absorption spectrum of HEAM crystal. **b** Tauc plot of HEAM crystal

3 Results and discussion

3.1 Single crystal X-ray diffraction

The HEAM crystallizes in the monoclinic space group $P2_1/c$ with unit cell parameters of $a = 4.246(10)$ Å, $b = 20.6998(6)$ Å, $c = 9.4184(3)$ Å and $\beta = 98(10)°$. CCDC.954038 contains the crystallographic information file (CIF) for the title compound. The charge transfer complex formed from the reaction of maleic acid with the ethanolamine, namely HEAM, $C_2H_8N_1O_1{}^{+}.C_4H_3O_4{}^{-}$, and the asymmetric unit consists of an ethanolamine in protonated form and a maleic acid in monoionized state. The molecular configuration and the atom numbering scheme of HEAM are shown in Fig. 3.

3.2 Ultraviolet–visible spectroscopy (UV–Vis)

The UV–Vis absorption spectrum (Fig. 4a) has the lower absorption edge at around 340 nm. The crystal is transparent in the entire visible region (400–800 nm) and can be useful for optical applications. The band gap can be assessed by the predominant mechanism of band to band transitions. The absorption coefficient (α) was calculated using

$$\alpha = \ln(1/T)d \quad (1)$$

where d is the thickness of the crystal in mm and T is the transmittance.

From the Tauc relation [14],

$$(\alpha h\nu) = A(h\nu - E_g)^n \quad (2)$$

where α is the absorption coefficient, ν is the frequency, h is Planck's constant, A is the proportionality constant, the band gap energy (E_g) has been calculated in turn by the extrapolation of the linear portion of the curve to a point $(\alpha h\nu)^2 = 0$, 'n' is the index that characterizes the optical absorption process. The energy gap value of 3.6 eV is found to be the predominant transition taking place in the material and is shown in Fig. 4b. Hence, the moderate band gap value represents the optimum laser threshold of the reported material.

3.3 Photoluminescence

Photoluminescence occurs when a system is excited to a higher energy level by absorbing a photon, and then spontaneously decays to a lower energy level, emitting a photon in the process. PL spectroscopy is a selective and extremely sensitive probe of discrete electronic state [15]. Input excitation wavelength is given by 340 nm and the corresponding emission spectrum is shown in Fig. 5. The intensity peak was centered at 433 nm and shows violet emission. The emission was attributed to electronic transition from σ* → n. Interestingly, the fluorescence emission is almost the mirror image of excitation spectrum for all of compounds [16].

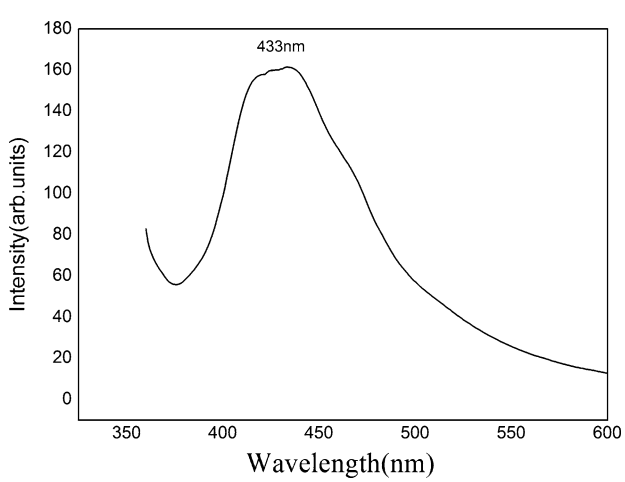

Fig. 5 Photoluminescence spectrum of HEAM

3.4 Z-scan study

Z-scan is a simple technique wherein the sample is moved along the Z-direction of a focused Gaussian laser beam (pulses) and the transmitted intensity is measured through a finite (or open) aperture in the far-field as a function of the sample position Z, measured with respect to the focal plane. As the sample traverses through the beam focus (at $Z = 0$), self-focusing or—defocusing modifies the wave front phase, thereby modifying the transmitted beam intensity. In the open aperture configuration, all the transmitted intensity is collected devoid of aperture and these data provided information about the nonlinear absorption processes in the sample. Figure 6a, b illustrate the open aperture data recorded for HEAM at two different peak intensities of ~165 and ~270 GW/cm^2, respectively, with signatures in both the scans indicating reverse saturation absorption (RSA). The open aperture Z-scan data generally depict RSA characteristics if (a) the excited state has strong absorption compared with that of the ground state (b) if the sample possesses two-photon absorption (2PA) or three-photon absorption (3PA). The Z-scan measurements were taken in ethanol solution using a 1-mm cuvette.

In particular, we observed 2PA and an effective 3PA with respect to the increasing peak intensity. 2PA process occurs when the material has an electronic excited level at twice the frequency ω of the input beam. Effective 3PA is a process wherein the photons reach excited state through two steps: 2PA followed by excited state absorption. In this case, the population resides in the excited state (after 2PA) for a short period of time before it is excited to higher energy levels. It could also involve 1 + 2 photon kind of absorption also. 2PA involves the imaginary part of $\chi^{(3)}$ and effective 3PA involves the imaginary part of $\chi^{(5)}$. A process involving the imaginary part of optical susceptibility implies damping of the wave in the medium resulting from the exchange of energy between the optical field and the medium. To determine the real part of $\chi^{(3)}$, we performed closed aperture Z-scan measurement to find the nonlinear refractive index (n_2). Figure 6c depicts the closed aperture data for the sample recorded at a peak intensity of ~69 GW/cm^2. The valley followed by peak indicates that the sample possesses positive type of nonlinearity and self-focusing behavior. Self-focusing occurs as a combined result of positive n_2, and a spatial variation of the laser intensity in which the beam is more intense at the center than at the edges.

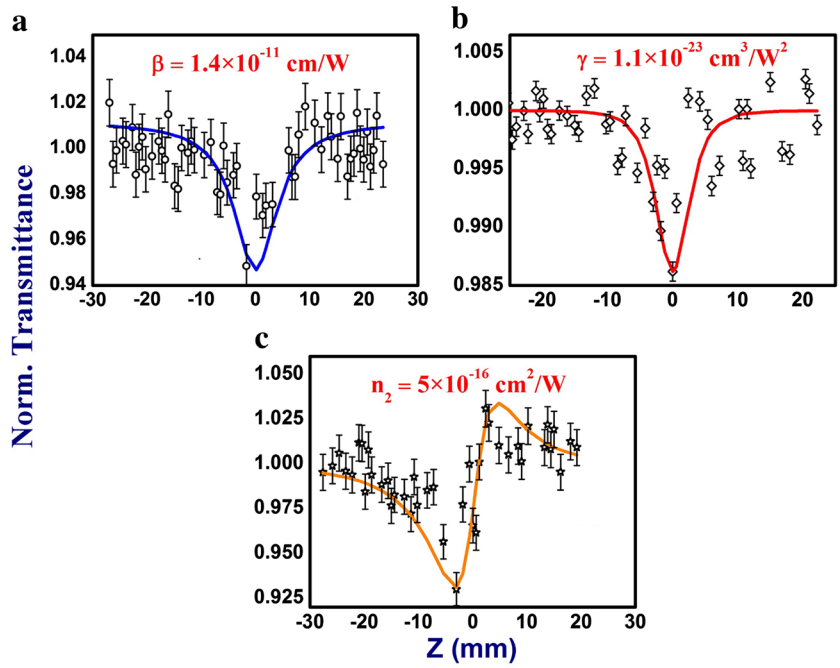

Fig. 6 Open aperture Z-scan data recorded for HEAM at (**a**) 165 GW/cm^2 and (**b**) 270 GW/cm^2 and (**c**) closed aperture Z-scan data obtained at I_{00} = 69 GW/cm^2

The open aperture data obtained were fitted for 2PA and 3PA. We combine the linear and two 2PA (β) (or) 3PA (γ) coefficients giving a total absorption coefficient [17] as

$$\alpha(I) = \alpha_0 + \beta I \tag{3}$$

$$\alpha(I) = \alpha_0 + \gamma I^2 \tag{4}$$

where α_0, β and γ are linear absorption, 2PA and 3PA coefficients, respectively. Equations (3) and (4), β and γ can be obtained by fitting the following equation

$$\frac{dI}{dz} = -\alpha(I)I \tag{5}$$

where z corresponds to the sample position and I is the excitation intensity ($I = I_{00}$ at $Z = 0$).

Assuming a spatial and temporal Gaussian profile for laser pulses the normalized energy transmittance for the process of nonlinear absorption [18] and the normalized open aperture Z-scan transmittance can be determined as follows [19]

$$T_{\mathrm{OA}} = \frac{\int_{-\infty}^{+\infty} P(t)dt}{\int_{-\infty}^{+\infty} P_i(t)dt} \tag{6}$$

where $P(t)$ is transmitted power through the sample and $P_i(t)$ is the initial power on the sample and the equation for 2PA open aperture nonlinear transmittance is given by [18, 20]

$$T_{\mathrm{OA}}(2\mathrm{PA}) = \frac{1}{\pi^{\frac{1}{2}} q_0(z,0)} \int_{-\infty}^{\infty} \left[1 + q_0(z,0)\exp\left(\tau^2\right)\right] d\tau \tag{7}$$

Three-photon absorption (3PA) equation is;

$$T_{\mathrm{OA}}(3\mathrm{PA}) = \frac{1}{\pi^{1/2} P_0} \int_{-\infty}^{\infty} \ln\left\{\left[1 + p_0^2 \exp\left(-2x^2\right)\right]^{1/2} + p_0 \exp\left(-x^2\right)\right\} dx \tag{8}$$

where $q_0(z,0) = \beta I(Z) L_{\mathrm{eff}}$, $p_0(z,0) = 2\gamma I^2(z) L'_{\mathrm{eff}} I(Z) = I_{00}/(1 + \frac{Z^2}{Z_0^2})$ is the excitation intensity at position Z and I_{00} is the peak intensity;$L_{\mathrm{eff}} = \frac{1-e^{-\alpha_0 L}}{\alpha_0}$ and $L'_{\mathrm{eff}} = \frac{1-e^{-2\alpha_0 L}}{2\alpha_0}$ where L is the sample length, β is 2PA coefficient, γ is 3PA coefficient, α_0 is linear absorption coefficient and Z_0 is the Rayleigh range.

If $q_0 < 1$ or $p_0 < 1$, Eq. (7) or (8) can be expanded in a Taylor series as

$$T_{\mathrm{OA}}(2\mathrm{PA}) = \sum_{m=0}^{\infty} (-1)^m \frac{q_0^m}{(m+1)^{3/2}} \tag{9}$$

$$T_{\mathrm{OA}}(3\mathrm{PA}) = \sum_{m=1}^{\infty} (-1)^{m-1} \frac{p_0^{2m-2}}{(2m-1)!(2m-1)^{1/2}} \tag{10}$$

Furthermore, if the higher order terms are ignored, we obtain:

$$T_{\mathrm{OA}}(2\mathrm{PA}) = 1 - \frac{\beta I_0 L_{\mathrm{eff}}}{2^{3/2}} \tag{11}$$

$$T_{\mathrm{OA}}(3\mathrm{PA}) = 1 - \frac{\gamma I_0^2 L'_{\mathrm{eff}}}{3^{3/2}} \tag{12}$$

These two expressions enable ones to identify 2PA or 3PA processes [21].

Table 1 Summary of nonlinear coefficients of HEAM

$\beta \times 10^{-12}$ (cm/W)	$n_2 \times 10^{-16}$ (cm^2/W)	$Im\lvert\chi^{(3)}\rvert \times 10^{-22}$ (m^2/V^2)	$Re\lvert\chi^{(3)}\rvert \times 10^{-22}$ (m^2/V^2)	$\lvert\chi^{(3)}\rvert \times 10^{-22}$ (SI)	$\lvert\chi^{(3)}\rvert \times 10^{-14}$ (e.s.u)
14	5	0.87535	4.9107	4.9881	3.5725

Table 2 Comparison of third-order nonlinear optical parameters with some known compounds

Compound name	$n_2 \times 10^{-16}$ cm^2/W	$\beta \times 10^{-12}$ (cm/W)	$Im\chi^{(3)} \times 10^{-22}$ (m^2/V^2)	$Re\chi^{(3)} \times 10^{-22}$ (m^2/V^2)	Type of laser, wavelength and pulses
4Br4MSP/ 4Cl4MSP	0.95	5	0.98	0.315	Ti:Sa, 800 nm, 2 ps [22]
4Br4MSP	2.30	5.5	0.046	2.27	Ti:Sa,800 nm, 2 ps [23]
3Br4MSP	2.00	3.8	0.047	1.98	Ti:Sa, 800 nm, 2 ps [23]
4N4MSP	2.40	4.0	0.097	2.36	Ti:Sa, 800 nm, 2 ps [23]
MMP	2.97	2.4	0.15	2.9	Ti:Sa, 800 nm, 2 ps [24]
BaF_2	3.07	60	1.52	3.66	Nd:YAG, 266 nm, 15 ps [25]
KTP	23	100	7.13	38.7	Nd:YAG, 532 nm, 22 ps [25]
BBO	3.64	10	0.38	5	Nd:YAG, 355 nm, 17 ps [25]
$LiNbO_3$	82	380	42.5	218	Nd:YAG, 532 nm, 22 ps [25]
BTMO	119	340	25.7	213	Nd:YAG, 532 nm, 5 ns [26]
HEAM	5	14	0.87535	4.9107	Ti:sa, 800 nm, 2 ps [Present]

Similarly, the normalized closed aperture transmittance can be determined as follows

$$T\left(\frac{z}{z_0}\right) = 1 - \frac{4\left(\frac{z}{z_0}\right)\Delta\phi_0}{\left[\left(\frac{z}{z_0}\right)^2+1\right]\left[\left(\frac{z}{z_0}\right)^2+9\right]} \tag{13}$$

where Z is the sample position, $z_0 = \pi\omega_0^2/\lambda$ is the Rayleigh range: ω_0 is the beam waist at the focal point ($Z = 0$), λ is the wavelength; $\Delta\phi_0$ is the nonlinear phase shift.

The difference between the peak and valley transmission (ΔT_{p-v}) written in terms of the on axis phase shift at the focus as,

$$\Delta\phi_0 = \frac{\Delta T_{p-v}}{0.406(1-S)^{0.25}} \tag{14}$$

where S(50 %) is the aperture linear transmittance and is calculated using $S = 1 - \exp(-2r_a^2/\omega_a^2)$; where r_a is the aperture radius and ω_a is the beam radius at the aperture.

The real and imaginary parts of the third-order nonlinear optical susceptibility ($\chi^{(3)}$) are defined as

$$Re|\chi^{(3)}|(m^2/V^2) = 2n_0^2 c\varepsilon_0 n_2 (m^2/W) \tag{15}$$

$$Im|\chi^{(3)}|(m^2/V^2) = (1/2\pi)n_0^2 c\varepsilon_0 \lambda\beta(m/W) \tag{16}$$

$$|\chi^{(3)}|(SI) = [(Re|\chi^{(3)}|)^2 + (Im|\chi^{(3)}|)^2]^{1/2} \tag{17}$$

where 'ε_0' is the vacuum permittivity, 'n_0' is the linear refractive index of the sample, and c is the velocity of light in vacuum.

The sign of nonlinear refraction n_2 was positive in our case. The best fit for n_2 of $\sim 5\times10^{-16}$ cm^2/W was obtained for HEAM using Eq. (13). The data presented in Fig. 6a, b and c open circles, diamonds, stars represent the experimental data for 2PA, 3PA and closed aperture, respectively, while the solid lines are the theoretical fits [9, 10, 17–20]. The values of β, γ, n_2 obtained from open and closed aperture Z-scan data were $\sim 10^{-11}$cm/W at 165 GW/cm^2, $\sim 10^{-23}$ cm^3/W^2 at 270 GW/cm^2 and $\sim 10^{-16}$ cm^2/W at 69 GW/cm^2, respectively. The obtained data are summarized in Table 1. Table 2 shows the comparison of HEAM data with the reported molecules. β and n_2 of HEAM demonstrated higher values compared to the reported chalcone derivatives such as (2E)-1-(4-bromophenyl)-3-[4-(methylsulfanyl) phenyl] prop-2-en-1-one/ (2E)-1-(4-chlorophenyl)-3-[4-(methyl sulfanyl) phenyl] prop-2-en-1-one (4Br4MSP/4Cl4MSP), (2E)-1-(4-bromophenyl)-3-[4(methylsulfanyl) phenyl] prop-2-en-1-one (4Br4MSP), (2E)-1-(3-bromophenyl)-3-[4-(methylsulfanyl) phenyl] prop-2-en-1-one (3Br4MSP), (2E)-3[4(methylsulfanyl) phenyl]-1-(4-nitrophenyl) prop-2-en-1-one

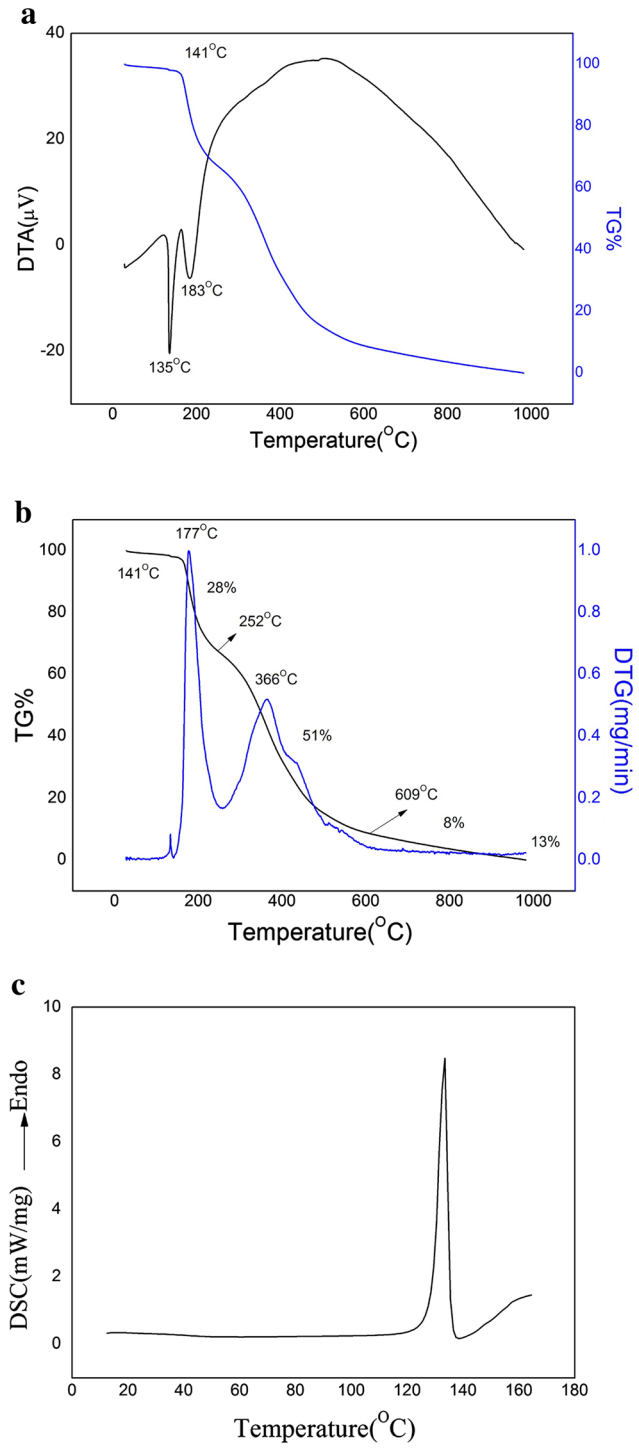

Fig. 7 **a** TG/DTA curve of HEAM crystal. **b** TG/DTG curve of HEAM crystal. **c** DSC curve of HEAM crystal

(4N4MSP) and 1-[4-({(E)-[4-(methylsulfanyl) phenyl] methylidene} amino)phenyl] ethanone (MMP) [22–24] and Beta barium borate (BBO) and Barium fluoride (BaF_2) [25]. However, lithium niobate ($LiNbO_3$), potassium titanyl phosphate (KTP) [25] and β-$BaTeMo_2O_9$ (BTMO) compounds [26] demonstrated higher β and n_2 value than

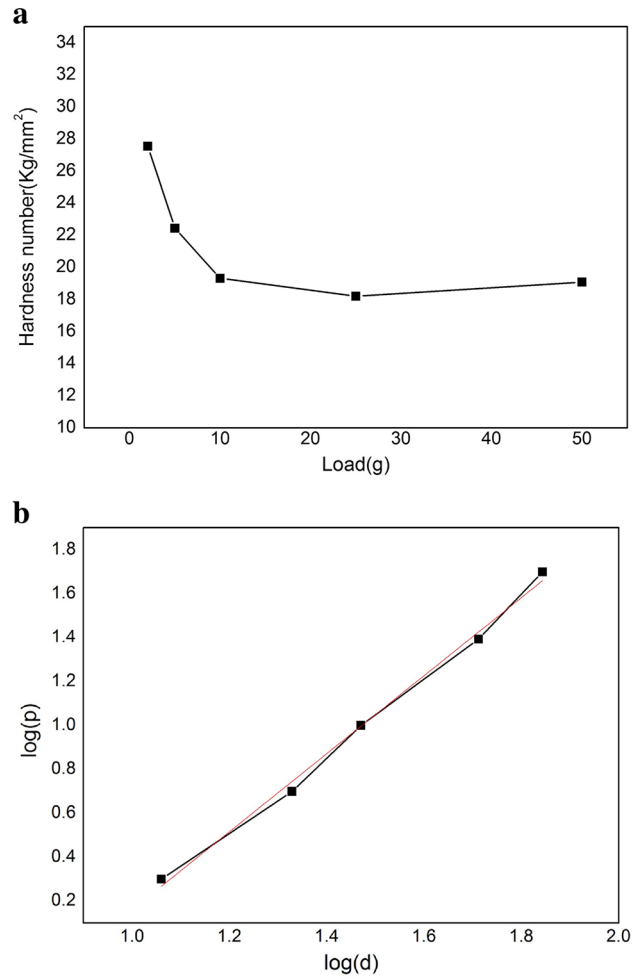

Fig. 8 **a** Load p versus H_v of HEAM crystal. **b** Log (d) versus Log (p) plot of HEAM crystal

HEAM sample. Third-order susceptibility varies with the type of laser, wavelength and pulses.

Maleic acid with relatively large π-conjugation forms crystalline maleate with ethanolamine molecules through extensive hydrogen bonding. Third-order nonlinearity is highly dependent on the number of double bonds and π electron conjugation length [27]. Hence, in the present work, double bond present in the maleic acid is responsible for the nonzero value of $\chi^{(3)}$. The third-order susceptibility was found to be $\sim 3.57 \times 10^{-14}$ e.s.u. The most important application of the observed 2PA and 3PA is in optical limiting devices. Optical power limiting is an area of growing interest due to its applications to eye and sensor protection against intense light [28, 29].

3.5 Thermal analysis

Fig. 7a and b show TG/DTA curve and derivative TG graphs of HEAM crystal. The thermal stability of the

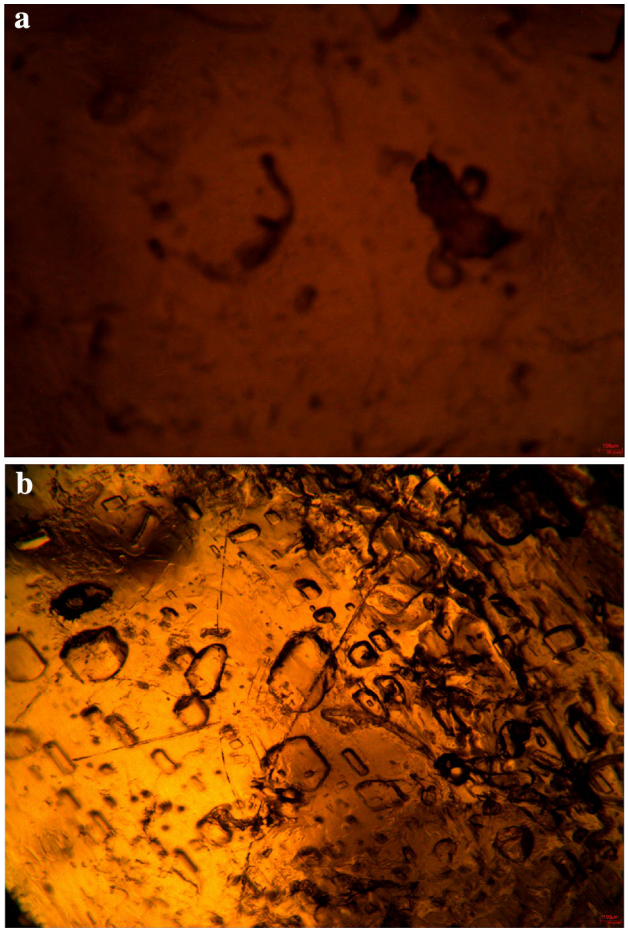

Fig. 9 **a** Surface of as-grown HEAM crystal. **b** Surface of HEAM crystal etched by ethanol for 50 s (Magnification: 10X)

compound was found to be 140 °C from the TG curve. As evident from DTG plot (Fig. 7b), the observation of two major peaks confirms the two stage weight loss. In the first stage decomposition, the weight loss of 26 % from 141 to 255 °C may be due to the release of carbon dioxide gas. The second stage decomposition occurs from 258 °C with the mass loss of 52 % followed by 8 % weight loss up to 1,000 °C. The residue left over at the end of the stage is 14 %. The DTA shows two endothermic peaks at 135 and 183 °C. The first sharp peak reveals the melting point of the title crystal which is in good agreement with DSC as shown in Fig. 7c. This sharp peak indicates the good crystallinity of the HEAM compound. The second peak at 183 °C was due to the decomposition of the sample which coincides exactly with the first stage decomposition curve of TG. The absence of decomposition up to 140 °C shows that the material can be useful for optical applications.

3.6 Vickers microhardness test

The measurement was made on (011) plane at room temperature and the loads of different magnitude such as 2,5,10, 25 and 50 g were applied with indentation time of 10 s. The Vicker's hardness number (H_V) is calculated using the relation,

$$H_V = 1.8544 \times \frac{P}{d^2}\ \text{kgm m}^{-2} \tag{18}$$

where 'P' is the applied load in kg and 'd' is the diagonal length in mm.

The variation of H_v with the applied load is shown in Fig. 8a. The Vickers microhardness decreases with applied load. The load of 50 g is sufficient to induce cracks on the crystal. The relation connecting the applied load (P) and diagonal length (d) of the indenter was given by Meyer's law $P = ad^n$. Here, 'n' is Meyer's index or work hardening coefficient. The work hardening coefficient was calculated using the least square fitting method and was found to be 1.77 and is shown in Fig. 8b. According to Onitsch [30], n lies between 1 and 1.6 for hard materials and the values are more than 1.6 for soft materials. The relatively strong interaction between the cationic and anionic planes or strong ionic bond between anion and cation pairs is responsible for the mechanical strength of HEAM crystals [31]. It is clear from the above analysis that the title crystal belongs to soft material category.

3.7 Etching study

The photograph was taken using polarizing optical microscope in reflection mode as shown in Fig. 9a and b. Etching of the crystal surface along (011) plane was carried out by dipping the crystal in ethanol for 10 s at room temperature. Before etching, no defined pattern of growth is visible, but after etching for 10 s, rectangular shaped etch pits are observed on the crystal surface. Results indicate that the crystal grown in the present study possesses moderate quality with medium etch pit density.

4 Conclusions

In this study, HEAM crystal was grown for the first time using slow evaporation method and found to crystallize in monoclinic system with centrosymmetric $P2_1/c$ space group. Optical studies revealed that the compound has absorption edge at 340 nm and is a violet emissive material. Thermal studies of the title compound reveals the melting point at 135 °C, and the thermal stability was up to 140 °C. Vickers microhardness indicates that the material can withstand up to 50 g. From the Z-scan analysis, HEAM

charge transfer complex exhibits RSA and self-focusing behavior. The third-order susceptibility was found to be of the order of 10^{-14} e.s.u. The Z-scan study reveals that the title compound has an adequate amount of third-order nonlinear property compared to some of the reported molecules. Hence, the title compound can be useful for optical limiting device applications.

Acknowledgments The author Dr. R. Nagalakshmi is thankful to Council of Scientific and Industrial Research (Sanction No: 03(1158)/10/EMR-II), New Delhi for the financial assistance under major research project and Ms.N.Sudharsana is thankful to CSIR for awarding JRF in this project. The authors are grateful to thank Dr. R. Justin Joseyphus, for thermal (TG/DTA) facility, Department of Physics, National Institute of Technology, Tiruchirappalli, India. The authors are thankful to Dr. P. Srinivasan, University College of Technology, Department of Physics, Panruti for extending the facility for UV–visible study. The authors are also thankful to SAIF, IIT Madras for the single crystal XRD and DSC measurements. Dr. S. Venugopal Rao thanks DRDO for financial support.

References

1. N.P. Porollo, Z.G. Aliev, G.I. Dzhardimalieva, I.N. Ivleva, I.E. Uflyand, A.D. Pomogailo, N.S. Ovanesyan, Russ. Chem. Bull. **46**, 362 (1997)
2. T. Mallik, T. Kar, Cryst. Res. Technol. **40**, 778 (2005)
3. M. Anbuchezhiyan, S. Ponnusamy, C. Muthamizhchelvan, Spectrochim. Acta **74A**, 917 (2009)
4. S. Natarajan, S.A.M. Britto, E. Ramachandran, Cryst. Growth Des. **6**, 37 (2006)
5. T. Mallik, T. Kar, Mater. Lett. **61**, 3826 (2007)
6. G. Anandha Babu, P. Ramasamy, J. Cryst. Growth **311**, 1185 (2009)
7. L. Vivien, N. Izard, D. Riehl, F. Hache, E. Anglaret, AIP Conf. Proc. **685**, 559 (2003)
8. Ch. Bosshard, K. Sutter, Ph. Pretre, J. Hulliger, M. Florsheimer, P. Kaatz, P. Gunter, *Organic Nonlinear Optical Materials, Advances in Nonlinear Optics* (Gordon and Breach, Switzerland, 1995)
9. D. Swain, A. Rana, P.K. Panda, S. Venugopal Rao, Chem. Phys. Lett. **610–611**, 310 (2014)
10. S. Venugopal Rao, T.S. Prashant, T. Sarma, P.K. Panda, D. Swain, S.P. Tewari, Chem. Phys. Lett. **514**, 98 (2011)
11. D. Swain, P.T. Anusha, T. Sarma, P.K. Panda, S. Venugopal Rao, Chem. Phys. Lett. **580**, 73 (2013)
12. P.T. Anusha, D. Swain, S. Hamad, T.S. Prashant, L. Giribabu, S.P. Tewari, S. Venugopal Rao, J. Phys. Chem. C **116**, 17828 (2012)
13. S. Venugopal Rao, J. Mod. Opt. **58**, 1024 (2011)
14. J. Tauc, *Amorphous and Liquid Semiconductors* (Plenum, New York, 1974), pp. 159–220
15. T.H. Gfroerer, in *Encyclopedia of Analytical Chemistry*, ed by R.A. Meyers, (Wiley, Chichester, 2000), pp. 9209–9231
16. Z.-L. Gong, Y.-S. Xie, B.-X. Zhao, H.-S. Lv, W.-Y. Liu, L.-W. Zheng, S. Lian, J. Fluoresc. **21**, 355 (2011)
17. M. Sheik-Bahae, A.A. Said, T.H. Wei, D.J. Hagan, E.W. Van Stryland, IEEE J. Quant. Electron. **26**, 760 (1990)
18. B. Gu, W. Ji, Opt. Exp. **16**, 10208 (2008)
19. D.S. Correa, L.D. Boni, L. Misoguti, I. Cohanoschi, F.E. Hernandez, C.R. Mendonca, Opt. Commu. **277**, 440 (2007)
20. K.V. Saravanan, K.C.J. Raju, M.G. Krishna, S.P. Tewari, S. Venugopal Rao, Appl. Phys. Lett. **96**, 232905 (2010)
21. J. He, Y. Qu, H. Li, J. Mi, W. Ji, Opt. Express **13**, 9235 (2005)
22. E.D. D'silva, G.K. Krishna Podagatlapalli, S. Venugopal Rao, D. Narayana Rao, S.M. Dharmaprakash, Cryst. Growth Des. **11**, 5362 (2011)
23. E.D. D'silva, G.K. Krishna Podagatlapalli, S. Venugopal Rao, D. Narayana Rao, S.M. Dharmaprakash, Mater. Res. Bull. **47**, 3552 (2012)
24. E.D. D'silva, G.K. Krishna Podagatlapalli, S. Venugopal Rao, D. Narayana Rao, S.M. Dharmaprakash, Opt. Laser Technol. **44**, 1689 (2012)
25. R. DeSalvo, A.A. Said, D.J. Hagan, E.W. Van Stryland, M. Sheik-Bahae, IEEE J. Quantum Electron. **32**, 1324 (1996)
26. I. Fuks-Janczarek, R. Miedzinski, M.G. Brik, A. Majchrowski, L.R. Jaroszewicz, I.V. Kityk, Solid State Sci. **27**, 30 (2014)
27. J.P. Hermann, J. Ducuing Hermann, J. Appl. Phys. **45**, 5100 (1974)
28. J.W. Perry, K. Mansour, I.-Y.S. Lee, X.-L. Wu, P.V. Bedworth, C.-T. Chen et al., Science **273**, 1533 (1996)
29. R.A. Ganeev, A.I. Ryasnyansky, M.K. Kodirov, R. Kamalov, R.I. Tugushev, T. Usmanov, Appl. Phys. B-Lasers O. **74**, 47 (2002)
30. E.M. Onitsch, Microskopie. **2**, 131 (1947)
31. A.S. Haja Hameed, S. Rohani, W.C. Yu, C.Y. Tai, C.W. Lan, J. Cryst. Growth **297**, 146 (2006)